

Geometry and Perception Guided Gaussians for Multiview-consistent 3D Generation from a Single Image

Pufan Li*
Wangxuan Institute of Computer
Technology, Peking University
Beijing, China
230112067@pku.edu.cn

Bi'an Du*
Wangxuan Institute of Computer
Technology, Peking University
Beijing, China
pkudba@stu.pku.edu.cn

Wei Hu
Wangxuan Institute of Computer
Technology, Peking University
Beijing, China
forhuwei@pku.edu.cn

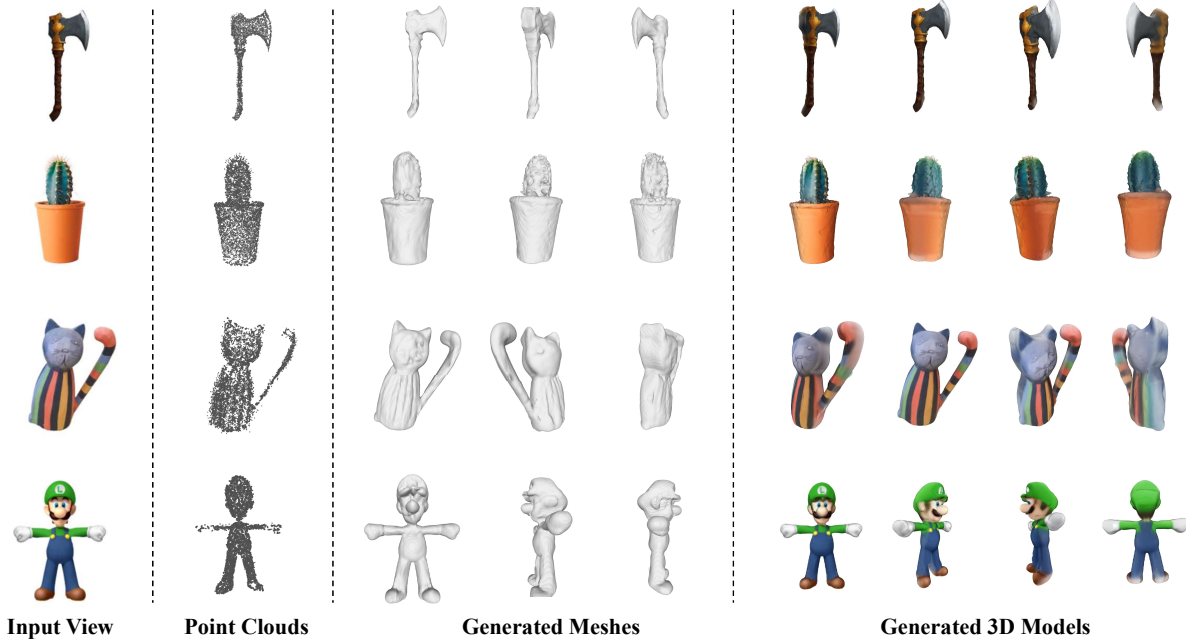


Figure 1: Our method is able to generate multiview-consistent 3D object from a single-view input image of arbitrary objects. For each input, our method can generate point clouds, meshes and images from any views without additional training.

ABSTRACT

Generating realistic 3D objects from single-view images requires natural appearance, 3D consistency, and the ability to capture multiple plausible interpretations of unseen regions. Existing approaches often rely on fine-tuning pretrained 2D diffusion models or directly generating 3D information through fast network inference or 3D Gaussian Splatting, but their results generally suffer from poor multiview consistency and lack geometric detail. To tackle these issues, we present a novel method that seamlessly integrates geometry and perception priors without requiring additional model training to reconstruct detailed 3D objects from a single image. Specifically, we train three different Gaussian branches initialized

from the geometry prior, perception prior and Gaussian noise, respectively. The geometry prior captures the rough 3D shapes, while the perception prior utilizes the 2D pretrained diffusion model to enhance multiview information. Subsequently, we refine 3D Gaussian branches through mutual interaction between geometry and perception priors, further enhanced by a reprojection-based strategy that enforces depth consistency. Experiments demonstrate the higher-fidelity reconstruction results of our method, outperforming existing methods on novel view synthesis and 3D reconstruction, demonstrating robust and consistent 3D object generation.

KEYWORDS

Single-view Generation, Geometry, Perception, Prior Knowledge, 3D Gaussian Splatting, Consistency

* Equal contribution. Pufan Li, Bi'an Du and Wei Hu are with Wangxuan Institute of Computer Technology, Peking University, No. 128, Zhongguancun North Street, Beijing, China. Corresponding author: Wei Hu.

ACM Reference Format:

Pufan Li*, Bi'an Du*, and Wei Hu. 2025. Geometry and Perception Guided Gaussians for Multiview-consistent 3D Generation from a Single Image. <https://doi.org/10.1145/nnnnnnnn.nnnnnnnn>

1 INTRODUCTION

Generating realistic 3D objects from single-view images requires that the resulting 3D content not only appears natural and consistent from all viewpoints, but also accounts for multiple plausible interpretations of unseen regions. Humans possess a remarkable ability to envision a complete 3D structure from a single image, even when certain parts of the object remain hidden. By drawing on prior knowledge of familiar objects, the human brain infers and represents missing regions to form a coherent 3D concept. In the fields of computer vision and graphics, substantial progress has been made in deriving implicit 3D representations from images [30, 40, 44]. However, explicitly reconstructing 3D objects directly from 2D images remains a formidable challenge.

Recent studies on single view 3D generation can be broadly classified into two main categories: 3D native approaches and optimization-based 2D lifting approaches. The former [8, 13, 16, 31, 32, 41] rely on large, manually annotated datasets and significant computational resources to train large-scale neural networks, thereby enabling efficient, 3D-consistent outputs at inference time. However, these methods still struggle to produce realistic details. Meanwhile, 2D diffusion models [14, 36] have shown remarkable capabilities in image generation, opening new possibilities for 3D tasks. SyncDreamer [25] and MVD-Fusion [15] extend 2D diffusion models to capture the joint probability distribution of multiview images, achieving satisfying novel view synthesis results. On the other hand, diffusion models can act as a bridge between 2D images and 3D objects. A prime example is Dreamfusion [33], which introduces Score Distillation Sampling (SDS) to distill 3D geometry and appearance from a pretrained 2D diffusion model. This SDS technique has become central to many recent 2D lifting methods, where it is often used to optimize Neural Radiance Fields (NeRF) [30], mitigating inconsistencies and ambiguities while modeling rich 3D content.

Compared to NeRF-based methods, 3D Gaussian Splatting [18] requires less memory to reconstruct 3D scenes. DreamGaussian [37] brings 3D Gaussian Splatting into the generative realm by using Score Distillation Sampling (SDS) to inject 2D prior knowledge into the 3D Gaussians, thus boosting generation efficiency while maintaining quality. However, its outputs still suffer from issues like blurry back views and oversaturated textures.

In this work, we propose a novel framework that seamlessly integrates geometry and perception priors to generate 3D objects from a single view, aiming to directly generating 3D consistent content while avoiding training or fine-tuning additional neural networks at high computational and time costs. Our method adopts 3D Gaussian Splatting as its 3D representation and enhances it with the geometry and perception prior knowledge, merely involving optimizing the parameters of the Gaussians. We initialize three different Gaussian branches from the geometry prior, perception prior and Gaussian noise, aiming to integrate the advantages of different initializations. By leveraging the perception prior to augment the input image, we infuse the Gaussians with richer multiview information beyond that of the single input image. Compared with previous Gaussian-based single-image-to-3D methods [37], our approach leverages on broader prior knowledge to refine the Gaussians.

Further, our method integrates different types of prior knowledge to address their respective limitations, by refining 3D Gaussian Splattings through mutual interaction. Specifically, we expand the SDS method to co-SDS that introduces the images from different Gaussian branches, which enables modeling a more accurate image distribution at certain perspective. We also propose a reprojection-based method to exploit the discrepancy between the projected positions and the actual observed pixel locations in the rendered images from different Gaussian branches, further enhancing the consistency of generated results.

In summary, our contributions are:

- We introduce a novel pipeline for single-image 3D object generation by integrating geometry and perception prior knowledge into Gaussian Splatting.
- We devise a mechanism that enables multiple Gaussians to interact, effectively merging priors from different domains. This interaction refines the 3D Gaussian branches and leads to more accurate representations.
- Experimental results on the Google Scanned Object [6] dataset demonstrate the superiority of our method compared to competing approaches.

2 RELATED WORK

2.1 Generative 3D Representation

A good 3D representation is important for most 3D tasks. Classic representations, including point clouds [7, 11], voxels [4, 27] and meshes [39, 43], offer detailed descriptions of geometry and appearance. However, they lack flexibility in the underlying topology and are difficult to optimize during the training process.

Neural Radiance Fields (NeRF) [30] is an advanced deep learning technique designed for 3D reconstruction [1, 20] and generation [21, 33]. By leveraging neural networks to implicitly model 3D scenes, it can produce high-quality 3D reconstructions and generate realistic novel view images from a limited set of 2D input images. However, this comes with challenges such as high computational costs and substantial data requirements. 3D Gaussian splatting [18] has emerged as a promising alternative to NeRF for 3D representation, which achieves smooth and continuous 3D scene representation through Gaussian distribution, showcasing remarkable improvements in both reconstruction quality and computational efficiency. DreamGaussian [37] for the first time adapts 3D Gaussian splatting into generation tasks, achieving fast processing speeds and convinced quality.

2.2 Diffusion Models for 3D Generation

Diffusion model [14, 36] have made significant achievements in the field of 2D image generation. For this reason, a series of works [9, 16, 26, 32] try to apply the diffusion model in 3D tasks to repeat the success in 2D. However, the paucity of 3D data poses a significant challenge for the direct training of diffusion models on such data. Despite some researchers' efforts to train 3D diffusion models using only 2D images, the generation quality remains significantly inferior to that of comparable 2D image generation models, exhibiting notably weaker generalization capability.

Many works [10, 28, 33, 37, 38, 45] resort to use a high-quality 2D diffusion model to build a bridge to connect 2D and 3D data,

which better promotes 3D inference, instead of directly training a 3D diffusion model. Dreamfusion [33] and SJC [38] formulate a "score distillation" objective that utilizes the 2D diffusion model as prior and distills the knowledge from a text-to-image pretrained diffusion model to generate 3D objects from texts. A series of subsequent works use score distortion to optimize the neural radiation field. RealFusion [28] achieves 360° 3D reconstruction from a single object image by leveraging a 2D diffusion model enhanced with text inversion for single-image adaptation. In contrast, NeuraLLift-360 [45] employs depth-aware NeRF and learns scene generation through denoising diffusion models. DreamGaussian [37] for the first time uses Score Distillation Sampling to optimize 3D Gaussian Splatting. Some impressive results had been achieved, which demonstrates the effectiveness of distillation from 2D diffusion model.

Some works fine-tune 2D diffusion models to make them better suited for 3D tasks. SparseFusion [47] propose a method of learning a novel perspective diffusion model, using an epipolar feature transformer to construct a perspective conditional feature model for sparse perspective reconstruction, and obtaining more accurate 3D reconstruction results through distillation techniques. Zero-1-to-3 [24] utilize a pretrained large-scale image diffusion model and fine-tune it to generate novel view images based on single-view input images. It has been proven that fine-tuning pretrained image diffusion models on large-scale 3D datasets can achieve better generalization ability. MVD-Fusion [15] and SyncDreamer [25] model the joint probability distribution of multiview images and used a 3D aware feature attention mechanism to synchronize the intermediate states of all generated images at each step of the reverse process, thereby associating corresponding features between different views which makes the generated multiview images more consistent.

2.3 Single Image to 3D Generation

Single image to 3D generation task aims to generate 3D content from a reference image. A recent class of approaches [24, 28, 47] reframes the task as learning conditional generation of novel views. Some efforts [2, 5, 12, 19] have been made to extend 2D diffusion models from single-view images to multiview images. By adapting large-scale pretrained generative models, these methods can learn generalizable view synthesis. However, most of these methods focus on image generation, which we think is not entirely equivalent to generating 3D content.

In our view, single-view to 3D generation should result in a detailed and visualized 3D content rather than just multiview images. Although multiview images provide a partial representation of the object or scene, they lack the comprehensive spatial understanding and interactivity that true 3D models offer. A complete 3D representation enables applications such as virtual reality, augmented reality, and 3D printing, where depth, texture, and geometry are crucial. Therefore, the ultimate goal should be to generate high-fidelity 3D models that capture fine-grained details, maintain structural consistency, and allow for seamless manipulation and rendering from any viewpoint. This requires not only advancements in multiview consistency but also innovations in 3D reconstruction techniques, such as implicit neural representations (e.g., NeRF) or explicit mesh-based methods, to bridge the gap between 2D inputs and fully realized 3D

outputs. We believe that tasks such as [4, 11, 27, 29] that directly train diffusion models to generate point clouds and voxels, or using generative Gaussian Splatting model with companion mesh extraction and texture refinement in UV space in DreamGaussian [37], are more suitable for single view 3D generation.

3 METHOD

In this section, we first provide the preliminaries on 3D Gaussian Splatting, diffusion models and SDS loss (Section 3.1). Then we introduce the consistency enhancement framework for single view 3D generation that combines geometrical and perceptual priors simultaneously (Section 3.2), where the core parts are how to fully use prior knowledge (Section 3.3) and further improve generation consistency (Section 3.4).

3.1 Preliminaries

3.1.1 3D Gaussian Splatting. 3D Gaussian Splatting [18] is an advanced technique in computer graphics and vision to efficiently represent and render complex 3D scenes. It enables fast and high-quality rendering through differentiable splatting operations. The method models 3D geometry and appearance using a set of anisotropic 3D Gaussian distributions. Each Gaussian is characterized by a set of parameters: a mean position $\mathbf{x} \in \mathbb{R}^3$, a scaling factor $\mathbf{s} \in \mathbb{R}^3$, a rotation quaternion $\mathbf{q} \in \mathbb{R}^4$ representing covariance, and attributes for color $\mathbf{c} \in \mathbb{R}^3$ and opacity $\alpha \in \mathbb{R}^3$. These parameters are collectively denoted as Θ , where the parameters of the i -th Gaussian are given by $\Theta_i = \{\mathbf{x}_i, \mathbf{s}_i, \mathbf{q}_i, \alpha_i, \mathbf{c}_i\}$.

To determine the color of each pixel \mathbf{p} in the image, a neural point-based rendering approach is employed. The rendering process proceeds as follows:

$$\mathbf{C}(\mathbf{p}) = \sum_{i \in \mathcal{N}} \mathbf{c}_i \alpha_i \prod_{j=1}^{i-1} (1 - \alpha_j), \quad (1)$$

where \mathcal{N} denotes the related Gaussians.

3.1.2 From Diffusion Model to SDS Loss. Diffusion models [14] excel in generating high-fidelity samples and have demonstrated great success in applications including image synthesis, super-resolution, and inpainting. Inspired by principles from non-equilibrium thermodynamics, these models transform a simple distribution (e.g., Gaussian noise) into a complex target distribution (e.g., natural images) through a sequence of iterative denoising steps. The diffusion framework consists of two primary components: a forward diffusion process and a corresponding reverse (denoising) process.

In the forward process, the initial data x_0 drawn from the data distribution $p(x)$ are progressively corrupted by introducing incremental noise in multiple time steps. This yields a sequence of increasingly noisy data points that eventually converge to pure noise. Mathematically, this forward diffusion is modeled as a Markov chain:

$$q(x_t | x_{t-1}) = \mathcal{N}(x_t; \sqrt{1 - \beta_t} x_{t-1}, \beta_t \mathbf{I}), \quad (2)$$

where x_t denotes the noisy data at timestep t , and β_t controls the noise schedule.

In the reverse process, the model learns to progressively remove noise from the corrupted data by reversing the forward diffusion. Specifically, a neural network is trained to estimate the noise introduced at each timestep, enabling the reconstruction of the original

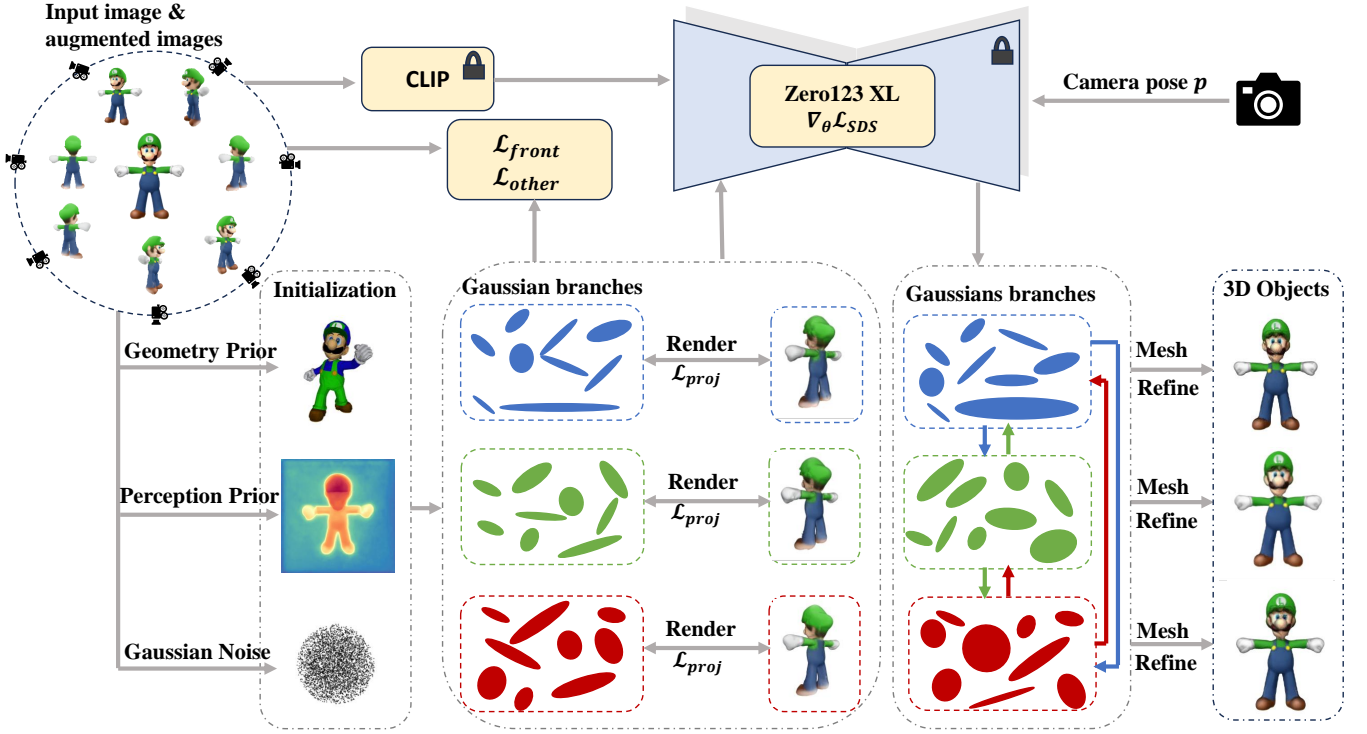


Figure 2: The network architecture of the proposed method. We use the geometry prior, perception prior and Gaussian noise to initialize three different Gaussian branches. At each training step, each Gaussian branch is supervised by the input image and augmented images generated by the perception prior. Meanwhile, a reprojection loss is employed to self-supervise the alignment of their corresponding image observations. To further explore the advantages of each Gaussian branch, we incorporate the proposed co-SDS loss to enhance the multiview consistency. We also refine Gaussian branches through mutual interaction including pseudo views co-regularization and untrusted-region mask. Finally, a mesh refine module [37] is adopted to obtain a textured mesh.

data from pure noise. Mathematically, this reverse diffusion is also formulated as a Markov chain:

$$p_{\theta}(x_{t-1} | x_t) = \mathcal{N}(x_{t-1}; \mu_{\theta}(x_t, t), \Sigma_{\theta}(x_t, t)), \quad (3)$$

where μ_{θ} and Σ_{θ} represent parameters learned by the neural network.

Directly applying 2D diffusion models to the 3D domain is challenging due to limited 3D data. DreamFusion [33] addresses this by introducing Score Distillation Sampling (SDS), an optimization method that leverages 2D diffusion priors for text-to-3D generation. Given a differentiable 3D model $f(\theta)$ capable of rendering images, SDS provides gradient guidance toward high-probability image regions conditioned on input y . The SDS loss gradient is defined as:

$$\nabla_{\theta} \mathcal{L}_{SDS} = \mathbb{E}_{t,p,\epsilon} \left[w(t) \left(\epsilon_{\phi}(x_t; y, t, \Delta p) - \epsilon \right) \frac{\partial x}{\partial \theta} \right], \quad (4)$$

where t is the timestep, x the rendered image, x_t its noisy latent at timestep t , $w(t)$ a weighting function, ϵ_{ϕ} the noise predicted by the 2D diffusion prior, and Δp the relative camera pose.

3.2 Overall Framework

We propose a novel framework for high-quality single-image-to-3D generation, as shown in Figure 2. Given a single image as input,

our goal is to accurately reconstruct the corresponding 3D object positioned at the origin, following the setting of [25]. 3D Gaussian Splatting is adopted as our 3D representation. We initialize 3 Gaussian branches with the geometry prior, perception prior and Gaussian noise. Each Gaussian branch is supervised by the input image and the augmented images generated by the perception prior. We incorporate mutual interaction including co-SDS, pseudo views co-regularization and untrusted-region mask to refine the 3 Gaussian branches. We also propose the reprojection loss to self-supervise the alignment of their corresponding image observations, further enhancing the consistency of generated results. Finally, we adopt a mesh refine module [37] to obtain a textured mesh.

3.3 Different Prior Knowledge Guidance

In this subsection, we analyze the role of different priors in improving generation quality. Specifically, we address challenges related to initializing and optimizing Gaussian representations. Unlike reconstruction tasks, structure-from-motion (SfM) methods cannot be applied due to having only a single input image. Additionally, optimization becomes challenging given only a frontal viewpoint, limiting the guidance available for Gaussian training.

3.3.1 Geometry Prior. Considering that extending the geometrical representation can achieve alignment between the geometrical data

and the CLIP embedding space [35]. The geometry prior can be acquired through retrieving structurally analogous 3D shapes from an external dataset, following [3], which chooses to incorporate external 3D prior information into text-to-3D generation by designing a shape supervision loss based on prior 3D shapes. However, it is crucial to recognize the inherent distinction between these two generation tasks: while text-to-3D generation emphasizes high-level semantic alignment with text descriptions, image-to-3D generation requires that the frontal perspective of the generated object is exactly the same as the provided image in pixel level. Directly applying 3D shape supervision loss may lead to conflicts between the input perspective and the generated perspective, so we use the retrieved 3D shapes to initialize Gaussian positions to ensure an accurate representation that is smoother, structurally consistent, and closely aligned with the target object.

Specifically, we use the recently released OpenShape[22] model, which scales up the 3D backbone to align with CLIP as our 3D retrieval module. The retrieved 3D shape provides coarse shape reference for the generation process.

3.3.2 Perception Prior. 2D diffusion models have demonstrated powerful capabilities in image generation. Zero-1-to-3 [24] fine-tunes diffusion models to synthesize arbitrary views of an object given only a single frontal view, while SyncDreamer [25] and MVD-Fusion [15] further extend this concept by modeling joint probability distributions of multiview images, enabling simultaneous multiview image generation.

Using these pre-trained 2D models, we generate corresponding multiview images from the input image to guide the subsequent 3D Gaussian optimization. Despite the fact that the generation of additional views alleviates problems such as back-view blur to a certain extent, the resulting sparse and low-quality synthetic images are insufficient for reliable structure-from-motion (SfM) reconstruction to obtain accurate point clouds and poses, which plays a crucial role in the initialization of 3D Gaussians.

Following [17], we consider to address this limitation by incorporating depth information. Specifically, we utilize Marigold [17] to estimate depth maps from both the input and generated multiview images and combine them, forming an initial point cloud to initialize the 3D Gaussian Splatting model, providing a good solution for initialization issues.

3.4 Integration of Different Gaussian branches

Similar to [37], we adopt a simpler initialization strategy, randomly sampling Gaussian positions within a sphere, using unit scaling, and zero rotation. While this approach lacks object-specific prior information, it remains generally effective for generating a broad variety of objects. Therefore, we finally use the geometry prior guidance, the perception prior guidance, and random Gaussian sampling strategy to initialize different Gaussian branches, respectively.

Each type of initialization brings unique advantages, motivating us to integrate beneficial aspects across different 3D Gaussian branches. We observe distinct behaviors among these Gaussian branches during iterative optimization, influenced not only by their initializations but also by ambiguities in the 3D-to-2D projection and the Gaussian densification process, particularly the creation

and initialization of new Gaussians via normal sampling. To improve generation quality, it is essential to identify and suppress inaccurate Gaussian components while integrating complementary strengths from different initializations. We introduce perceptual augmentation loss and co-SDS loss to enhance the multiview consistency of the model.

Meanwhile, we incorporate reprojection loss \mathcal{L}_{proj} , a classical computer vision metric that quantifies the accuracy of projecting 3D points onto the 2D image plane. It reflects how well the reconstructed 3D points align with their corresponding image observations. Leveraging this property, we use the reprojection error to guide the alignment of local depth information in the 3D Gaussians, thereby enhancing the overall consistency of our model.

3.4.1 Perceptual Augmentation Loss. Specifically, we denote that the input image is \tilde{I}_R^0 with a foreground mask \tilde{I}_A^0 , the generated multiview images and their foreground masks are \tilde{I}_R^i and \tilde{I}_A^i where $i > 0$. For each 3D Gaussian branch, we optimize the reference view image I_R^0 and transparency I_A^0 to align with the input:

$$\mathcal{L}_{front} = \lambda_1 \|\tilde{I}_R^0 - I_R^0\|_2^2 + \lambda_2 \|\tilde{I}_A^0 - I_A^0\|_2^2. \quad (5)$$

The augmented image is not as good as the input image in terms of quality and credibility, so we cannot fully use pixel by pixel mean square error as the loss. Therefore, we add an additional D-SSIM term:

$$\mathcal{L}_{other} = \lambda_3 \|\tilde{I}_R^i - I_R^i\|_2^2 + \lambda_4 \|\tilde{I}_A^i - I_A^i\|_2^2 + \lambda_5 \mathcal{L}_{D-SSIM}(\tilde{I}_R^i, I_R^i), \quad (6)$$

for $i > 0$.

3.4.2 Co-SDS Loss. The SDS loss mentioned in Section 3.1 introduces noise to images rendered by 3D Gaussian Splatting from multiple perspectives and subsequently estimates the noise in the perturbed images using the input perspective as a conditional guide. This mechanism enables the 3D representation to align with the image distribution corresponding to the given perspective. At each step, we sample a random camera pose p orbiting the center of the object and render the RGB image I_R^p of the current view. Similar to DreamGaussian [37], we decrease the timestep t linearly during training, which is used to weight the random noise ϵ added to the rendered RGB image. Then different 2D diffusion priors ϕ can be used to optimize the underlying 3D Gaussians through SDS. We extend the SDS loss to jointly denoise images rendered from three Gaussian branches, formulated as:

$$\nabla_{\theta} \mathcal{L}_{SDS} = \mathbb{E}_{t,p,\epsilon} [w(t) (\epsilon_{\phi} (I_{R,t}^{1,p}, I_{R,t}^{2,p}, I_{R,t}^{3,p}; I_R^0, t, \Delta p) - \epsilon) \frac{\partial I_R^{1,p} I_R^{2,p} I_R^{3,p}}{\partial \theta}]. \quad (7)$$

Simultaneously introducing the image rendered from two other 3D Gaussian branches at this perspective to estimate noise is expected to enable the model to model a more accurate image distribution at this perspective.

3.4.3 Reprojection Loss for Depth Consistency. After projecting 3D spatial points onto the image plane, a discrepancy often exists between the projected positions and the actual observed pixel locations in the image. We aim to exploit this discrepancy as a supervisory signal to refine the 3D Gaussian branches, thereby promoting local geometric consistency of the 3D representation.

To this end, we sample a pair of views with minimal viewpoint difference, enabling us to approximate local correspondences across views and effectively guide the optimization process. Their camera extrinsic parameters are $\mathbf{M}_1 \in \mathbb{R}^{4 \times 4}$ and $\mathbf{M}_2 \in \mathbb{R}^{4 \times 4}$ from which we can get rotation and translation information of both views. For view 1, the rotation matrix is $\mathbf{R}_1 = \mathbf{M}_{1,[0:3,0:3]}^{-1}$ and the translation vector is $\mathbf{T}_1 = \mathbf{M}_{1,[0:3,3]}^{-1}$, \mathbf{R}_2 and \mathbf{T}_2 are in the same manner. With camera intrinsic matrix $\mathbf{K} \in \mathbb{R}^{3 \times 3}$, we need to calculate the corresponding position of each pixel of view 1 in view 2. For pixel $\mathbf{u} = (x, y, 1)^T \in \mathbb{R}^{3 \times 1}$ where x, y represent the row and column index, we first transform it to the world coordinate system:

$$(w_x, w_y, w_z)^T = \mathbf{R}_1^{-1}(\mathbf{K}^{-1}\mathbf{S}\mathbf{u} - \mathbf{T}_1), \quad (8)$$

where S is the scaling factor. Then we convert the point in the world coordinate system to another view:

$$\mathbf{u}' = S^{-1}\mathbf{K}(\mathbf{R}_2(w_x, w_y, w_z)^T + \mathbf{T}_2), \quad (9)$$

assert $T_1 = T_2 = T$, then we obtain:

$$\mathbf{u}' = \mathbf{K}\mathbf{R}_2\mathbf{R}_1^{-1}\mathbf{K}^{-1}\mathbf{u} + S^{-1}\mathbf{K}(\mathbf{1} - \mathbf{R}_2\mathbf{R}_1^{-1})\mathbf{T}, \quad (10)$$

the scale factor can be approximated as infinite, the Eq. 10 can be approximated as:

$$\mathbf{u}' = \mathbf{K}\mathbf{R}_2\mathbf{R}_1^{-1}\mathbf{K}^{-1}\mathbf{u}. \quad (11)$$

Through the above deduction, we can determine the corresponding position \mathbf{u}' of pixel \mathbf{u} from view 1 in view 2. We aim for the projected image to closely resemble the image rendered by the 3D Gaussian in view 2. Based on this, we design the depth consistency loss that the L2 norm between the estimated pixel values and the actual pixel values. It can be formulated as:

$$\mathcal{L}_{proj} = \frac{1}{|D_2|} \sum_{\mathbf{u} \in D_2} \|D_2(\mathbf{u}) - D_2(\mathbf{u}')\|_2^2, \quad (12)$$

where D_2 is the rendered depth image of 3D Gaussians in view 2 and $|D_2|$ means the total pixels of depth image.

3.4.4 Pseudo views co-regularization & Untrusted-Region Mask. Besides co-SDS, we also interact with different Gaussian branches through pseudo views co-regularization and untrusted-region mask. Please check the supplementary materials for more details.

3.5 Training Strategy

Given an input image, we perform several pre-processing steps to initialize the Gaussian branches:

First, we leverage a retrieval-based approach to identify the most similar 3D object from a reference dataset, which serves as the initialization for the first 3D Gaussian branch. Second, we utilize 2D priors to synthesize multiple novel views of the input image. For each generated view, we apply a monocular depth estimation model to infer depth maps, which are subsequently converted into point clouds. These point clouds are used to initialize the second 3D Gaussian branch.

During the first stage of optimization, we jointly refine both Gaussian branches using the following losses: a front-view alignment loss \mathcal{L}_{front} , an auxiliary multiview supervision loss \mathcal{L}_{other} , a local projection consistency loss \mathcal{L}_{proj} , and the gradient of the

Score Distillation Sampling loss $\nabla_{\theta}\mathcal{L}_{SDS}$. The overall objective at this stage is:

$$\mathcal{L}_1 = \mathcal{L}_{front} + \mathcal{L}_{other} + \alpha_1\mathcal{L}_{proj} + \nabla_{\theta}\mathcal{L}_{SDS}. \quad (13)$$

In the second stage of optimization, we introduce co-regularization using pseudo views and apply a pruning strategy based on untrusted-region masks. The final objective function becomes:

$$\mathcal{L} = \mathcal{L}_1 + \mathcal{L}_{co}. \quad (14)$$

4 EXPERIMENTS

4.1 Experimental Setup

4.1.1 Evaluation dataset. We adopt the Google Scanned Object [6] dataset as the evaluation dataset. We select the same 30 objects following [25] which consists of high-quality scanned items from daily objects to animals. For each object, we render 16 views with a size of 256×256 evenly spaced in azimuth from an elevation of 30 degrees and choose one of them as the input image.

4.1.2 Baseline. For novel view synthesis task, we adopt Zero123 [24], RealFusion [28], SyncDreamer [25], DreamGaussian [37] and MVD-Fusion [15] as baseline methods. Given an input image of an object and target view parameters, Zero123 can estimate the images of the target views. RealFusion is based on Stable Diffusion [36] and the SDS loss for single-view reconstruction. SyncDreamer and MVDFusion can generate multiview images simultaneously based on a fine-tuned 2D diffusion model. DreamGaussian adopts 3D Gaussian Splatting as its 3D representation and only uses input image and SDS loss to optimize the object without training additional models.

For single view reconstruction task, we adopt Zero123 [24], RealFusion [28], Magic123 [34], One-2-3-45 [23], Point-E [32], Shap-E [16], DreamGaussian [37], SyncDreamer [25] and MVDFusion [15] as baseline methods. Magic123 combines Zero123 with RealFusion to further improve the quality of the reconstruction. One-2-3-45 directly regresses the SDFs from the output images of Zero123. Point-E and Shap-E are 3D generative models trained on a large internal OpenAI 3D dataset, both of which are able to convert a single-view image into a point cloud or a shape encoded in an MLP. For Point-E, we convert the generated point clouds to SDFs for shape reconstruction. We should note that the diffusion-based methods require additional methods to render or distill objectives (e.g. Zero-1-to-3 requires an additional SDS distillation to generate 3D shapes whereas SyncDreamer relies on training Neus or NeRF).

4.1.3 Metrics. Compared to 2D tasks, it is hard to find a perfect indicator to measure the quality of 3D generation because of the diversity of 3D data. For novel view synthesis task, we adopt commonly used metrics: PSNR, SSIM[42], and LPIPS[46]. For single view reconstruction task, We report the commonly used Chamfer Distances (CD) and Volume IoU between ground-truth shapes and reconstructed shapes.

4.2 Novel View Synthesis

For this task, the quantitative results are shown in Table 1 and the qualitative results are shown in Figure 3. RealFusion[28] applies a

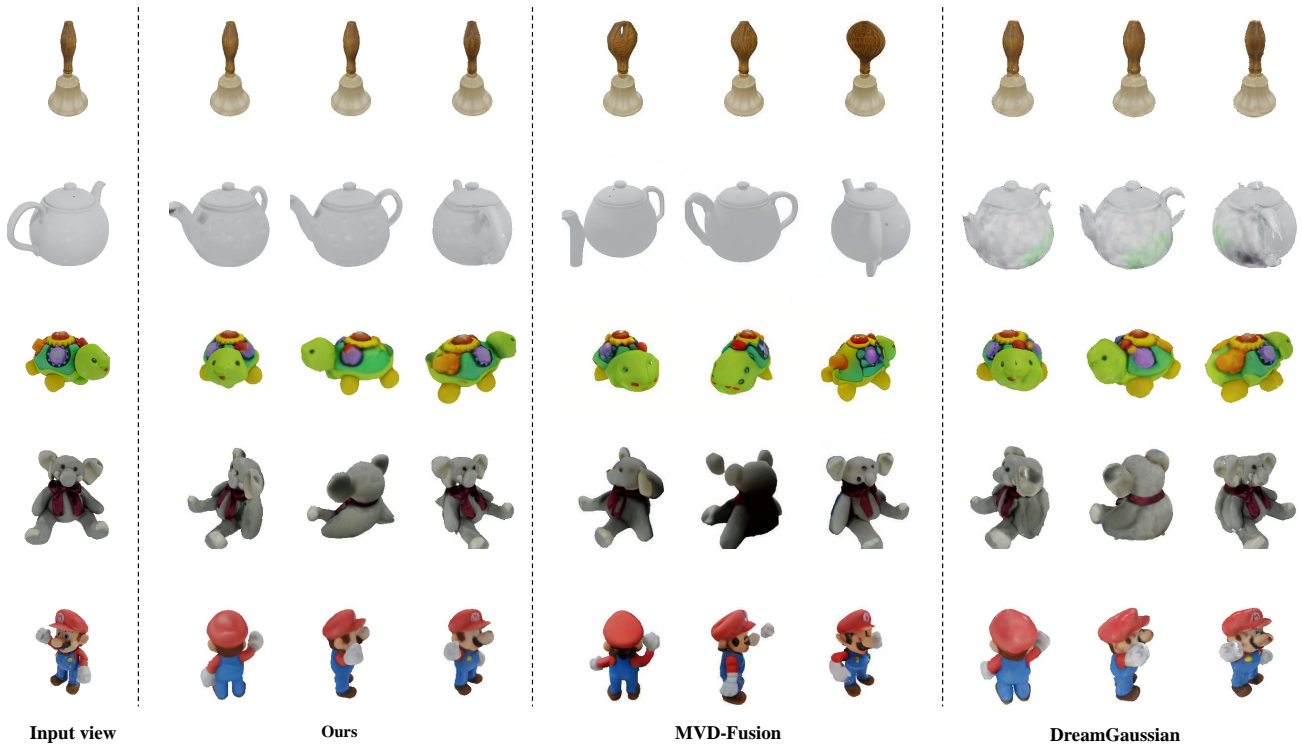


Figure 3: Qualitative comparison with MVD-Fusion and DreamGaussian on synthesized multiview images.

Table 1: The quantitative comparison in novel view synthesis. We report PSNR, SSIM, LPIPS on the GSO[6] dataset.

Method	PSNR \uparrow	SSIM \uparrow	LPIPS \downarrow
RealFusion [28]	15.26	0.722	0.283
Zero123 [24]	18.93	0.779	0.166
SyncDreamer [25]	20.05	0.798	0.146
MVD-Fusion [15]	19.99	0.830	0.159
DreamGaussian [37]	18.45	0.808	0.189
Ours	21.16	0.855	0.133

NeRF model to distill the stable diffusion model, but is unable to produce visually plausible images. Zero123[24] produces visually reasonable images but suffers from inconsistency and instability among the generated images. SyncDreamer[25] and MVD-Fusion[15] introduce the 3D attention mechanism to model the joint distribution of target views, enhancing the consistency of generation. However, both are limited to specific perspective. DreamGaussian[37] employs SDS loss to optimize Gaussians, achieving superior efficiency. However, there is only supervision from the frontal perspective, leading to blurring of non-frontal parts of the object. Our method fully utilizes geometry and perception prior knowledge to supervise different Gaussian branches, achieving competitive generation quality. From the testing perspective, the images show excellent geometry and perception consistency.

Table 2: The quantitative comparison in 3D reconstruction. We report Chamfer Distance and Volume IoU on the GSO dataset.

Method	Chamfer Distance \downarrow	Volume IoU \uparrow
Realfusion [28]	0.0819	0.2741
Magic123 [34]	0.0516	0.4528
One-2-3-45 [23]	0.0629	0.4086
Point-E [32]	0.0426	0.2875
Shape-E [16]	0.0436	0.3584
Zero123 [24]	0.0339	0.5035
SyncDreamer [25]	0.0261	0.5421
MVD-Fusion [15]	0.0310	-
DreamGaussian [37]	0.0327	0.5828
Ours	0.0189	0.6104

4.3 Single-view Reconstruction

For this task, we show the quantitative results in Table 2 and the qualitative comparison in Fig 4. Magic123[21] heavily relies on the estimated depth values of the input view, leading to incorrect results and instability. Point-E[32] and Shap-E[16] tend to produce incomplete meshes. One-2-3-45[23] reconstructs meshes from the outputs of Zero123, but the reconstruction suffers from loss of details due to image quality constraints. SyncDreamer uses vanilla NeuS[40] for reconstruction. The method is incapable of direct

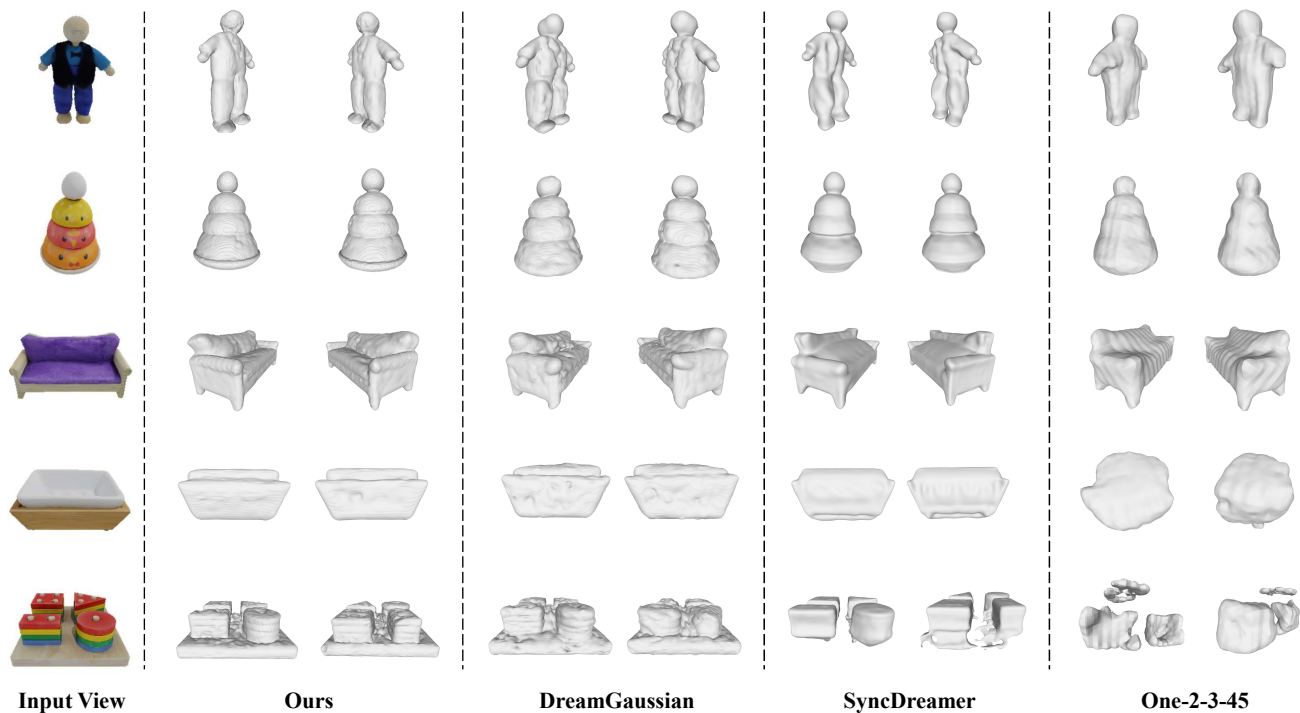


Figure 4: Qualitative comparison of reconstruction from single view images with different methods.

Table 3: The impact of different branches on novel view synthesis task.

Branch	PSNR \uparrow	SSIM \uparrow	LPIPS \downarrow
3D Shape Retrieval	20.74	0.846	0.144
Depth Estimation	20.75	0.849	0.142
Noise	20.63	0.847	0.144
All	21.16	0.855	0.133

3D mesh generation. Even with other methods, its texture quality still cannot reach the ideal standard. MVD-Fusion can directly obtain the point cloud but cannot generate meshes. Comparative evaluations demonstrate that our approach significantly improves reconstruction fidelity while simultaneously maintaining surface continuity while preserving high-frequency geometric features.

4.4 Ablation Study

In this section, we conduct a set of studies to verify the effectiveness of our designs.

4.4.1 Different Branches. To show how different Gaussian branches affect the result and the improvement of interactions in branches, we conduct experiments with only one of the three Gaussian branches without interactions (e.g. Co-SDS). As we can see in Table 3, only one branch shows a decrease in three indicators, demonstrating the necessity of the interaction of different branches. We speculate that training only one Gaussian branch may ignore the shortcoming of initialization. Taking the 3D Shape Retrieval branch as an example, it has the geometry prior but lacks the perception prior which

Table 4: The impact of different module on novel view synthesis task.

Module	PSNR \uparrow	SSIM \uparrow	LPIPS \downarrow
w/o Perception Augmentation Loss	20.62	0.844	0.147
w/o Co-SDS Loss	20.68	0.847	0.140
w/o Reprojection Loss	20.95	0.851	0.136
All	21.16	0.855	0.133

misses some perspective information during the optimization process. Meanwhile, the co-SDS module cannot be implemented, which limits the distribution of images from a specific perspective.

4.4.2 Different Modules. To show how different modules mentioned in Sec. 3.4 affect the generation. We discard perceptual augmentation loss, co-SDS loss and reprojection loss respectively. As we can see in Table 4, the absence of any module will result in a decrease in effectiveness, proving the effectiveness of the three modules.

5 CONCLUSION

We present a novel method for reconstructing detailed 3D objects from a single image. Our method employs Gaussian splatting, guided by geometry and perception priors, to address the challenges of high memory requirements. Additionally, we refine Gaussian Splatting through mutual interaction between geometry and perception priors, further enhanced by a reprojection-based strategy that enforces depth consistency. Our approach achieves higher-fidelity reconstruction results, proving its versatility and applicability.

REFERENCES

- [1] Jonathan T Barron, Ben Mildenhall, Dor Verbin, Pratul P Srinivasan, and Peter Hedman. 2022. Mip-nerf 360: Unbounded anti-aliased neural radiance fields. In *Proceedings of the IEEE/CVF conference on computer vision and pattern recognition*. 5470–5479.
- [2] Eric R Chan, Koki Nagano, Matthew A Chan, Alexander W Bergman, Jeong Joon Park, Axel Levy, Miika Aittala, Shalini De Mello, Tero Karras, and Gordon Wetzstein. 2023. Generative novel view synthesis with 3d-aware diffusion models. In *Proceedings of the IEEE/CVF International Conference on Computer Vision*. 4217–4229.
- [3] Cheng Chen, Xiaofeng Yang, Fan Yang, Chengzeng Feng, Zhoujie Fu, Chuan-Sheng Foo, Guosheng Lin, and Fayao Liu. 2024. Sculpt3d: Multi-view consistent text-to-3d generation with sparse 3d prior. In *Proceedings of the IEEE/CVF Conference on Computer Vision and Pattern Recognition*. 10228–10237.
- [4] Christopher B Choy, Danfei Xu, JunYoung Gwak, Kevin Chen, and Silvio Savarese. 2016. 3d-r2n2: A unified approach for single and multi-view 3d object reconstruction. In *Computer vision—ECCV 2016: 14th European conference, amsterdam, the netherlands, October 11–14, 2016, proceedings, part VIII 14*. Springer, 628–644.
- [5] Congyue Deng, Chiyu Jiang, Charles R Qi, Xinchen Yan, Yin Zhou, Leonidas Guibas, Dragomir Anguelov, et al. 2023. Nerdi: Single-view nerf synthesis with language-guided diffusion as general image priors. In *Proceedings of the IEEE/CVF conference on computer vision and pattern recognition*. 20637–20647.
- [6] Laura Downs, Anthony Francis, Nate Koenig, Brandon Kinman, Ryan Hickman, Krista Reymann, Thomas B McHugh, and Vincent Vanhoucke. 2022. Google scanned objects: A high-quality dataset of 3d scanned household items. In *2022 International Conference on Robotics and Automation (ICRA)*. IEEE, 2553–2560.
- [7] Bi'an Du, Xiang Gao, Wei Hu, and Xin Li. 2021. Self-contrastive learning with hard negative sampling for self-supervised point cloud learning. In *Proceedings of the 29th ACM International Conference on Multimedia*. 3133–3142.
- [8] Bi'an Du, Xiang Gao, Wei Hu, and Renjie Liao. 2024. Generative 3d part assembly via part-whole-hierarchy message passing. In *Proceedings of the IEEE/CVF Conference on Computer Vision and Pattern Recognition*. 20850–20859.
- [9] Bi'an Du, Wei Hu, and Renjie Liao. 2024. Multi-scale Latent Point Consistency Models for 3D Shape Generation. *arXiv preprint arXiv:2412.19413* (2024).
- [10] Bi'an Du, Lingbei Meng, and Wei Hu. 2024. AugGS: Self-augmented Gaussians with Structural Masks for Sparse-view 3D Reconstruction. *arXiv e-prints* (2024), arXiv–2408.
- [11] Haoqiang Fan, Hao Su, and Leonidas J Guibas. 2017. A point set generation network for 3d object reconstruction from a single image. In *Proceedings of the IEEE conference on computer vision and pattern recognition*. 605–613.
- [12] Jiatao Gu, Alex Trevithick, Kai-En Lin, Joshua M Susskind, Christian Theobalt, Lingjie Liu, and Ravi Ramamoorthi. 2023. Nerfdiff: Single-image view synthesis with nerf-guided distillation from 3d-aware diffusion. In *International Conference on Machine Learning*. PMLR, 11808–11826.
- [13] Anchit Gupta, Wenhan Xiong, Yixin Nie, Ian Jones, and Barlas Oğuz. 2023. 3dgen: Triplane latent diffusion for textured mesh generation. *arXiv preprint arXiv:2303.05371* (2023).
- [14] Jonathan Ho, Ajay Jain, and Pieter Abbeel. 2020. Denoising diffusion probabilistic models. *Advances in neural information processing systems* 33 (2020), 6840–6851.
- [15] Hanzhe Hu, Zhizhuo Zhou, Varun Jampani, and Shubham Tulsiani. 2024. Myd-fusion: Single-view 3d via depth-consistent multi-view generation. In *Proceedings of the IEEE/CVF Conference on Computer Vision and Pattern Recognition*. 9698–9707.
- [16] Heewoo Jun and Alex Nichol. 2023. Shap-e: Generating conditional 3d implicit functions. *arXiv preprint arXiv:2305.02463* (2023).
- [17] Bingxin Ke, Anton Obukhov, Shengyu Huang, Nando Metzger, Rodrigo Caye Daudt, and Konrad Schindler. 2024. Repurposing diffusion-based image generators for monocular depth estimation. In *Proceedings of the IEEE/CVF Conference on Computer Vision and Pattern Recognition*. 9492–9502.
- [18] Bernhard Kerbl, Georgios Kopanas, Thomas Leimkühler, and George Drettakis. 2023. 3d gaussian splatting for real-time radiance field rendering. *ACM Trans. Graph.* 42, 4 (2023), 139–1.
- [19] Jiabao Lei, Jiapeng Tang, and Kui Jia. 2022. Generative scene synthesis via incremental view inpainting using rgb-d diffusion models. *CoRR* (2022).
- [20] Zhaoshuo Li, Thomas Müller, Alex Evans, Russell H Taylor, Mathias Unberath, Ming-Yu Liu, and Chen-Hsuan Lin. 2023. Neuralangelo: High-fidelity neural surface reconstruction. In *Proceedings of the IEEE/CVF Conference on Computer Vision and Pattern Recognition*. 8456–8465.
- [21] Chen-Hsuan Lin, Jun Gao, Luming Tang, Towaki Takikawa, Xiao-hui Zeng, Xun Huang, Karsten Kreis, Sanja Fidler, Ming-Yu Liu, and Tsung-Yi Lin. 2023. Magic3d: High-resolution text-to-3d content creation. In *Proceedings of the IEEE/CVF conference on computer vision and pattern recognition*. 300–309.
- [22] Minghua Liu, Ruoxi Shi, Kaiming Kuang, Yinhao Zhu, Xuanlin Li, Shizhong Han, Hong Cai, Fatih Porikli, and Hao Su. 2023. Openshape: Scaling up 3d shape representation towards open-world understanding. *Advances in neural information processing systems* 36 (2023), 44860–44879.
- [23] Minghua Liu, Chao Xu, Haian Jin, Linghao Chen, Mukund Varma T, Zexiang Xu, and Hao Su. 2023. One-2-3-45: Any single image to 3d mesh in 45 seconds without per-shape optimization. *Advances in Neural Information Processing Systems* 36 (2023), 22226–22246.
- [24] Ruoshi Liu, Rundi Wu, Basile Van Hoorick, Pavel Tokmakov, Sergey Zakharov, and Carl Vondrick. 2023. Zero-1-to-3: Zero-shot one image to 3d object. In *Proceedings of the IEEE/CVF international conference on computer vision*. 9298–9309.
- [25] Yuan Liu, Cheng Lin, Zijiao Zeng, Xiaoxiao Long, Lingjie Liu, Taku Komura, and Wenping Wang. 2023. Syncdreamer: Generating multiview-consistent images from a single-view image. *arXiv preprint arXiv:2309.03453* (2023).
- [26] Shitong Luo and Wei Hu. 2021. Diffusion probabilistic models for 3d point cloud generation. In *Proceedings of the IEEE/CVF conference on computer vision and pattern recognition*. 2837–2845.
- [27] Daniel Maturana and Sebastian Scherer. 2015. Voxnet: A 3d convolutional neural network for real-time object recognition. In *2015 IEEE/RSJ international conference on intelligent robots and systems (IROS)*. IEEE, 922–928.
- [28] Luke Melas-Kyriazi, Iro Laina, Christian Rupprecht, and Andrea Vedaldi. 2023. Refusion: 360deg reconstruction of any object from a single image. In *Proceedings of the IEEE/CVF conference on computer vision and pattern recognition*. 8446–8455.
- [29] Lars Mescheder, Michael Oechsle, Michael Niemeyer, Sebastian Nowozin, and Andreas Geiger. 2019. Occupancy networks: Learning 3d reconstruction in function space. In *Proceedings of the IEEE/CVF conference on computer vision and pattern recognition*. 4460–4470.
- [30] Ben Mildenhall, Pratul P Srinivasan, Matthew Tancik, Jonathan T Barron, Ravi Ramamoorthi, and Ren Ng. 2021. Nerf: Representing scenes as neural radiance fields for view synthesis. *Commun. ACM* 65, 1 (2021), 99–106.
- [31] Norman Müller, Yawar Siddiqui, Lorenzo Porzi, Samuel Rota Buló, Peter Kotschieder, and Matthias Nießner. 2023. Diffrr: Rendering-guided 3d radiance field diffusion. In *Proceedings of the IEEE/CVF Conference on Computer Vision and Pattern Recognition*. 4328–4338.
- [32] Alex Nichol, Heewoo Jun, Prafulla Dhariwal, Pamela Mishkin, and Mark Chen. 2022. Point-e: A system for generating 3d point clouds from complex prompts. *arXiv preprint arXiv:2212.08751* (2022).
- [33] Ben Poole, Ajay Jain, Jonathan T Barron, and Ben Mildenhall. 2022. Dreamfusion: Text-to-3d using 2d diffusion. *arXiv preprint arXiv:2209.14988* (2022).
- [34] Guocheng Qian, Jinjie Mai, Abdullah Hamdi, Jian Ren, Aliaksandr Siarohin, Bing Li, Hsin-Ying Lee, Ivan Skorokhodov, Peter Wonka, Sergey Tulyakov, et al. 2023. Magic123: One image to high-quality 3d object generation using both 2d and 3d diffusion priors. *arXiv preprint arXiv:2306.17843* (2023).
- [35] Alec Radford, Jong Wook Kim, Chris Hallacy, Aditya Ramesh, Gabriel Goh, Sandhini Agarwal, Girish Sastry, Amanda Askell, Pamela Mishkin, Jack Clark, et al. 2021. Learning transferable visual models from natural language supervision. In *International conference on machine learning*. PmlR, 8748–8763.
- [36] Robin Rombach, Andreas Blattmann, Dominik Lorenz, Patrick Esser, and Björn Ommer. 2022. High-resolution image synthesis with latent diffusion models. In *Proceedings of the IEEE/CVF conference on computer vision and pattern recognition*. 10684–10695.
- [37] Jiaxiang Tang, Jiawei Ren, Hang Zhou, Ziwei Liu, and Gang Zeng. 2023. Dream-gaussian: Generative gaussian splatting for efficient 3d content creation. *arXiv preprint arXiv:2309.16653* (2023).
- [38] Haochen Wang, Xiaodan Du, Jiahao Li, Raymond A Yeh, and Greg Shakhnarovich. 2023. Score jacobian chaining: Lifting pretrained 2d diffusion models for 3d generation. In *Proceedings of the IEEE/CVF conference on computer vision and pattern recognition*. 12619–12629.
- [39] Nanyang Wang, Yinda Zhang, Zhuwen Li, Yanwei Fu, Wei Liu, and Yu-Gang Jiang. 2018. Pixel2mesh: Generating 3d mesh models from single rgb images. In *Proceedings of the European conference on computer vision (ECCV)*. 52–67.
- [40] Peng Wang, Lingjie Liu, Yuan Liu, Christian Theobalt, Taku Komura, and Wenping Wang. 2021. Neus: Learning neural implicit surfaces by volume rendering for multi-view reconstruction. *arXiv preprint arXiv:2106.10689* (2021).
- [41] Tengfei Wang, Bo Zhang, Ting Zhang, Shuyang Gu, Jianmin Bao, Tadas Baltrusaitis, Jingjing Shen, Dong Chen, Fang Wen, Qifeng Chen, et al. 2023. Rodin: A generative model for sculpting 3d digital avatars using diffusion. In *Proceedings of the IEEE/CVF conference on computer vision and pattern recognition*. 4563–4573.
- [42] Zhou Wang, Alan C Bovik, Hamid R Sheikh, and Eero P Simoncelli. 2004. Image quality assessment: from error visibility to structural similarity. *IEEE transactions on image processing* 13, 4 (2004), 600–612.
- [43] Chao Wen, Yinda Zhang, Zhuwen Li, and Yanwei Fu. 2019. Pixel2mesh++: Multi-view 3d mesh generation via deformation. In *Proceedings of the IEEE/CVF international conference on computer vision*. 1042–1051.
- [44] Yiheng Xie, Towaki Takikawa, Shunsuke Saito, Or Litany, Shiqin Yan, Numair Khan, Federico Tombari, James Tompkin, Vincent Sitzmann, and Srinath Sridhar. 2022. Neural fields in visual computing and beyond. In *Computer Graphics Forum*, Vol. 41. Wiley Online Library, 641–676.
- [45] Dejia Xu, Yifan Jiang, Peihao Wang, Zhiwen Fan, Yi Wang, and Zhangyang Wang. 2023. Neurrallift-360: Lifting an in-the-wild 2d photo to a 3d object with 360deg views. In *Proceedings of the IEEE/CVF Conference on Computer Vision and Pattern*

- Recognition*. 4479–4489.
- [46] Richard Zhang, Phillip Isola, Alexei A Efros, Eli Shechtman, and Oliver Wang. 2018. The unreasonable effectiveness of deep features as a perceptual metric. In *Proceedings of the IEEE conference on computer vision and pattern recognition*. 586–595.
- [47] Zhizhuo Zhou and Shubham Tulsiani. 2023. Sparsefusion: Distilling view-conditioned diffusion for 3d reconstruction. In *Proceedings of the IEEE/CVF Conference on Computer Vision and Pattern Recognition*. 12588–12597.